Journal of Applied Electrochemistry (2005) 35:27–32
DOI 10.1007/s10800-004-2052-y

A sealed, starved-electrolyte nickel–iron battery

B. HARIPRAKASH[1], S.K. MARTHA[1], M.S. HEGDE[1] and A.K. SHUKLA[1,2,*]
[1]*Solid State and Structural Chemistry Unit, Indian Institute of Science, Bangalore 560 012, India*
[2]*Also at Central Electrochemical Research Institute, Karaikudi 630006, India*
*(*Author for correspondence, tel.: ++91-80-22932795, fax: ++91-80-23601310, e-mail: shukla@sscu.iisc.ernet.in)*

Received 03 March, 2004; accepted in revised form 17 July 2004

Key words: faradaic efficiency, float-charge, H_2–O_2 recombinant catalyst, Nickel–iron battery

Abstract

A sealed, starved-electrolyte, negative-limited 6 V/1 Ah laboratory prototype of a nickel–iron (Ni–Fe) battery comprising five cells stacked in series with ceria-supported platinum as hydrogen–oxygen recombinant catalyst was assembled. The battery was tested under various operational conditions. While a continuous increase in gaseous pressure in the cells was observed without the recombinant catalyst, the cells with the recombinant catalyst registered a decline in gaseous pressure subsequent to the onset of hydrogen–oxygen recombination. The battery showed little decay in its capacity during its life-cycle tests conducted at C/5 rate at 25 °C. The battery performance is superior to its conventional vented-counterpart.

1. Introduction

The nickel–iron (Ni–Fe) battery was independently developed by Edison in the US and Jünger in Sweden in 1901 [1, 2]. The battery is based on use of nickel oxyhydroxide (NiOOH) at the positive electrode and iron at the negative electrode. The charge–discharge reactions for the Ni–Fe battery are as follows:

$$2\mathrm{NiOOH} + \mathrm{Fe} + 2\mathrm{H_2O} \underset{\text{charge}}{\overset{\text{discharge}}{\rightleftharpoons}} 2\mathrm{Ni(OH)_2} + \mathrm{Fe(OH)_2} \qquad (E_{\text{cell}} = 1.37\,\text{V}) \quad (1)$$

During the discharge of a Ni–Fe cell with negative-limited configuration, the discharge reaction (1) further proceeds in a second step, at a potential lower than the first step as,

$$\mathrm{NiOOH} + \mathrm{Fe(OH)_2} \underset{\text{charge}}{\overset{\text{discharge}}{\rightleftharpoons}} \mathrm{Ni(OH)_2} + \mathrm{FeOOH} \qquad (E_{\text{cell}} = 1.05\,\text{V}) \quad (2)$$

The cell reactions are highly reversible in the alkaline electrolyte, particularly if the discharge is limited to the first step [3–8]. The Ni–Fe battery is an attractive system by virtue of its long charge–discharge cycle-life (typically 3000 cycles corresponding to a calendar life of about 20 years) even under adverse operational conditions such as over-charge, over-discharge, charge-stand, discharge-stand, and inadequate maintenance [3–16].

Between 1910 and 1960, Ni–Fe battery was widely used for traction applications. The interest in the battery waned from 1960 but was revived again around 1975, particularly for electric vehicle applications. The developmental work on Ni–Fe battery eventually faded with the advent of new battery chemistries. Historically, alkaline Ni–Fe secondary batteries have been developed and tested extensively in the US, Japan, Europe and the former Soviet Union with good results. However, a factor that limited the widespread applications of the battery was that it could not be made sealed and maintenance-free.

As a part of our ongoing research programme on Ni–Fe batteries [17–19], in this communication, we report a maintenance-free, starved-electrolyte Ni–Fe battery, which employs an efficient hydrogen-oxygen recombinant catalyst in its vent plug. The electrochemical performance parameters of the sealed Ni–Fe battery are superior in relation to the vented starved Ni–Fe battery. It is hoped that this study will rejuvenate R&D activities on secondary Ni–Fe batteries, which are both environmentally more benign and cost-effective among the nickel-based rechargeable batteries. The battery is ideally suited for applications in off-shore platforms and petrochemical industries. To our knowledge, this is the first study of its type on Ni–Fe cells/batteries.

2. Experimental

Iron active material obtained by vacuum decomposition of iron oxalate at 500 °C [20] comprises Fe and Fe_3O_4. Iron electrodes from this active material were obtained as follows. The active material was suspended in

10 wt% aq. KOH solution in required amounts and mixed in an ultrasonic agitator with 10 wt% powdered graphite, 1 wt% Bi_2S_3 and 0.5 wt% $NiSO_4$. To this slurry, 6 wt% polytetrafluroethylene (PTFE)-GP2 Fluon suspension was added drop-by-drop with thorough mixing. The resulting putty-like mass was rolled against a smooth steel plate. The rolled sheet of the active material with additives was folded around a degreased nickel mesh (dimensions: 6.5 mm × 5 mm × 1 mm) and compacted at an optimum compaction pressure of 675 kg cm^{-2} for 5 min. The roll-compacted electrodes were heat treated in a stream of nitrogen at 350 °C for 30 min [17]. The thickness of the finished electrodes was about 1.5 mm.

Iron electrodes thus prepared were inserted into pockets made from polypropylene separator-cloth, which were subjected to formation cycles in a flooded formation tank containing 6 M aq. KOH with 1 wt% LiOH as electrolyte with nickel-plaque counter electrodes placed on the either side of an iron electrode. The iron electrodes were found to form within 2–3 charge/discharge cycles [18]. During the first formation cycle, the electrodes were charged at C/20 rate followed by C/10 rate during the subsequent cycles. The electrodes were discharged at the C/5 rate during their formation.

Negative-limited Ni–Fe cells were assembled by stacking an iron electrode in between two sintered nickel-positive electrodes. The cells were housed in plexiglass containers in starved-electrolyte configuration, and were sealed with a plug containing 0.5 g of 2 at.% Pt/CeO_2 hydrogen–oxygen recombinant catalyst mixed with an equal amount of fumed silica. 6 V/1 Ah sealed, starved-electrolyte Ni–Fe batteries were assembled in a plexiglass container comprising five compartments to house the constituent Ni–Fe cells connected in series.

The recombinant catalyst was synthesized by a novel solution-combustion method as described elsewhere [21, 22]. In brief, the combustion mixture comprised ceric ammonium nitrate [$(NH_4)_2Ce(NO_3)_6$], chloroplatinic acid (H_2PtCl_6) and oxalyldihydrazide ($C_2H_2N_4O_2$) in the molar ratios 0.98:0.02:2.35. Oxalyldihydrazide derived from diethyl oxalate, and hydrazine hydrate acts as the fuel. Initially, 10 g of ceric ammonium nitrate (E-Merck India, 99.9% purity), 0.193 g of chloroplatinic acid (Ranbaxy Laboratories India, 99% purity), and 5.175 g of oxalyldihydrazide were dissolved in a minimum volume of water in a borosilicate glass dish. Subsequently, the borosilicate glass dish containing the redox mixture and an appropriate quantity of hydrazine hydrate was introduced into a muffle furnace maintained at 350 °C. The solution was found to froth and foam with concomitant loss of water. When the removal of water was complete, the redox mixture ignited with the flame temperature at ca. 1000 °C yielding a voluminous and finely dispersed ceria-supported platinum catalyst as a solid product within about 5 min. Powder X-ray diffraction (XRD) pattern of the 2 at% Pt/CeO_2 catalyst thus prepared was obtained on a Siemens D-5005 X-ray Diffractometer using CuK_α-radiation at a scan rate of $2°min^{-1}$.

Provision was also made to measure the pressure of the gases evolved from cells employing a BOURDON SEDEME (France), pressure transducer while charging the cells between C/5 and C rates. A chromel–alumel thermocouple was embedded in the catalyst-bed to monitor its temperature during the charge–discharge operations of the Ni–Fe cells. Galvanostatic charge–discharge tests at different rates between C/10 and C, and at temperatures ranging between 40 and −20 °C were conducted using AUTOLAB PGSTAT30 (EcoChemie, Utrecht, The Netherlands) fitted with a BSTR10A current booster module. The cells and batteries were also subjected to cycle-life studies. The battery was also subjected to continuous overcharging for 100 h at C/10 rate to evaluate the efficiency of the recombinant catalyst. Aforesaid experiments were also conducted on vented Ni–Fe cells/batteries.

3. Results and discussion

The powder XRD pattern for the as prepared 2 at.% Pt/CeO_2 catalyst is shown in Figure 1. The XRD pattern agrees well with CeO_2 in fluorite structure. The XRD pattern is devoid of any diffraction lines due to Pt-metal particles or oxides of platinum. This catalyst is highly stable in strong aq. KOH environment. Hydrogen–oxygen recombination efficiency of the catalyst is found to be nearly 100% and the recombination mechanism has been explained elsewhere [23].

Typical galvanostatic charge–discharge data obtained at C/5 rate for the catalyst-equipped starved-electrolyte Ni–Fe cell at 25 °C are shown in Figure 2. The cell offers a faradaic efficiency of about 60 at C/5 rate operation. However, the faradaic efficiency is about 70 and 80% at C/10 and C/20 rates, respectively. Rate-dependent capacity measurements on the Ni–Fe cell were also conducted at 25 °C, and the discharge

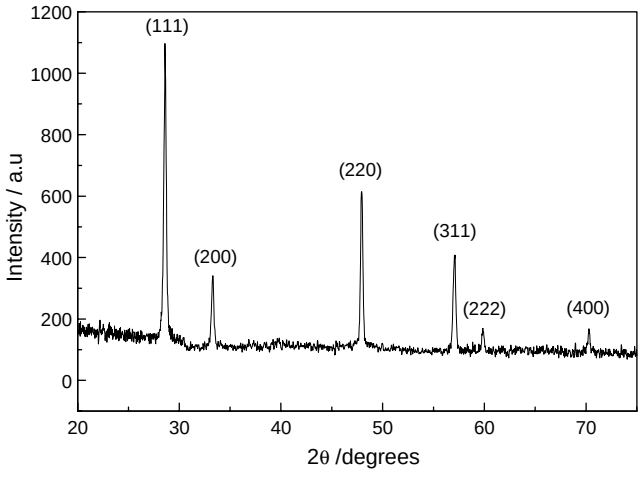

Fig. 1. Powder XRD pattern of the 2 at.% Pt/CeO_2 catalyst.

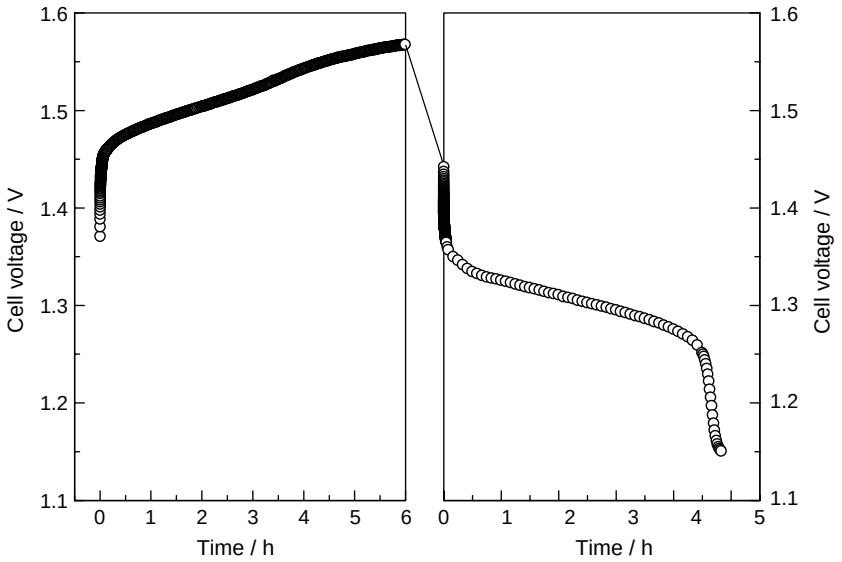

Fig. 2. A typical C/5 rate galvanostatic charge–discharge data for the 1.2 V/1 Ah starved-electrolyte sealed Ni–Fe cell at 25 °C.

capacity relative to the observed nominal capacity at C/5 rate are depicted in Figure 3. The cell delivers 62 and 125% of its nominal capacity at C and C/10 rates, respectively. Temperature-dependent discharge capacity measurements on the Ni–Fe cell were also conducted, and the data relative to its nominal capacity at C/5 rate at 25 °C are shown in Figure 4. At 40 °C, the cell delivered about 97% of the nominal capacity, which is due to its enhanced self-discharge at this temperature [24, 25]. The cell delivered only about 12% of the nominal capacity at −20 °C. The reduced capacity at low temperatures is due to decreased solubility of the reaction intermediates, as also due to increased resistance and viscosity of the electrolyte in conjunction with the retarded reaction kinetics at the electrodes [3, 4].

Pressure build-up data inside the Ni–Fe cell with and without catalyst while charging the cells at C/5 rate are shown in Figure 5. In Figures 6 and 7, variations in the internal pressure of the cell and catalyst-bed temperature as a function of cell charging rates at 25 °C are shown. From the data in Figure 6, it is seen that the pressure of the gases evolved while charging the cell rises initially and attains a maximum of 110 k N m^{-2} depending on its charging rate. Pressure inside the cell decreases after the onset of hydrogen–oxygen recombination. The data in Figure 7 suggest that the initial rise in the catalyst-bed temperature is due to the recombination of the hydrogen and oxygen gases evolved during the charging of the Ni–Fe cell. The catalyst-bed temperature stays between 45 and 65 °C depending on the charging rate of the cell.

The cells were subjected to charge-stand for 15 days to study their self-discharge characteristics, and the discharge data subsequent to the charge-stand are shown in

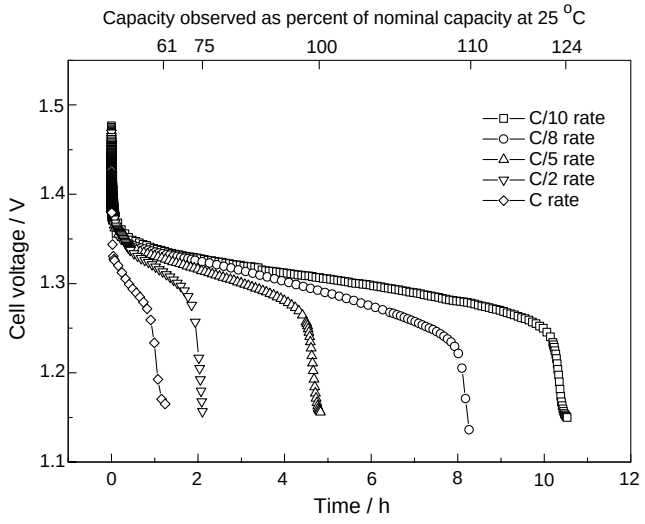

Fig. 3. Rate dependent performance characteristics of the 1.2 V/1 Ah starved-electrolyte sealed Ni–Fe cell obtained at 25 °C.

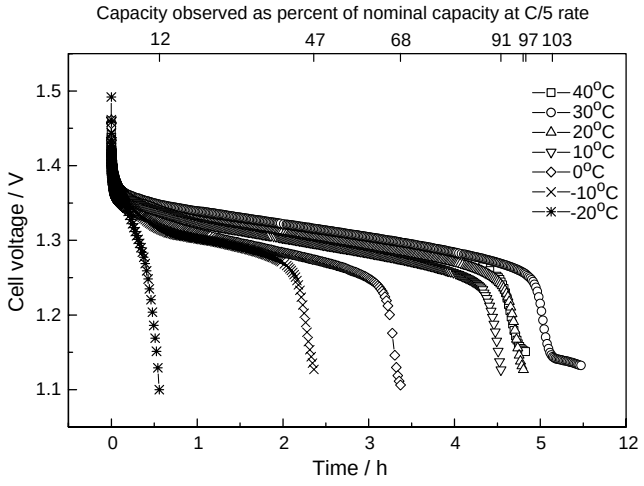

Fig. 4. Temperature dependent performance characteristics of the 1.2 V/1 Ah starved-electrolyte sealed Ni–Fe cell obtained at C/5 rate.

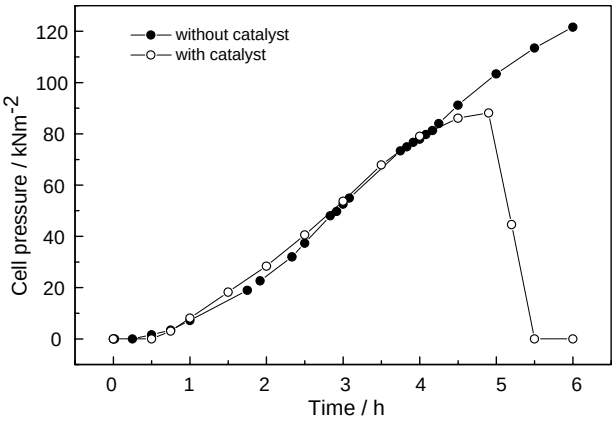

Fig. 5. Gas-pressure build up (in relation to atmospheric pressure) inside the cell with and without catalyst while charging the 1.2 V/1 Ah starved-electrolyte sealed Ni–Fe cell at C/5 rate at 25 °C.

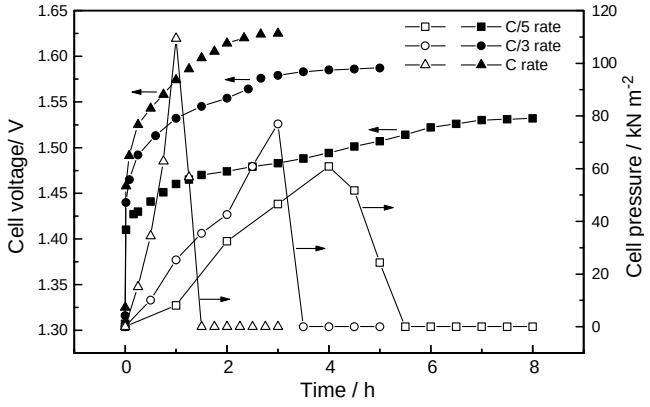

Fig. 6. Internal gas-pressure (in relation to atmospheric pressure) observed while charging the 1.2 V/1 Ah starved-electrolyte sealed Ni–Fe cell at different rates at 25 °C.

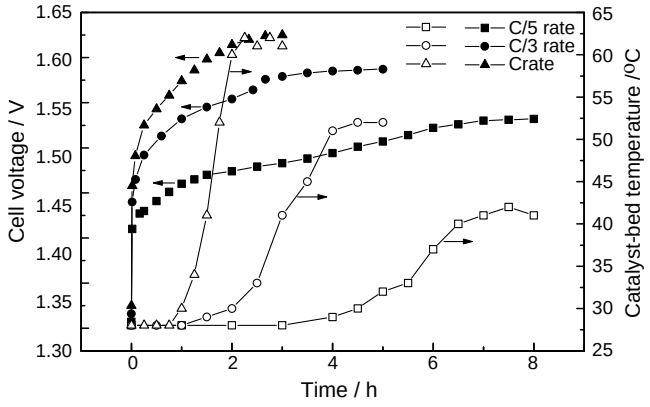

Fig. 7. Catalyst-bed temperature observed while charging the 1.2 V/1 Ah starved-electrolyte sealed Ni–Fe cell at different rates at 25 °C.

Figure 8 along with the discharge data subsequent to its immediate charge. The data suggest that the self-discharge rate of the cell to be 1.5% of its nominal capacity per day at 25 °C [26]. A higher initial drop during cell discharge subsequent to the charge-stand

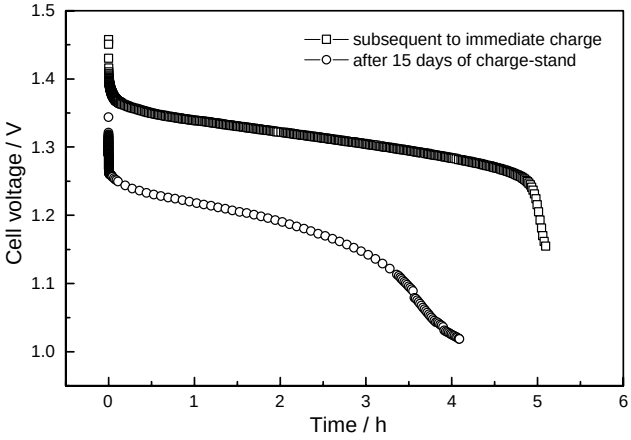

Fig. 8. Capacity retention data for the 1.2 V/1 Ah starved-electrolyte, sealed Ni–Fe cell.

suggests a build-up in the internal resistance of the cell due to the formation of $Fe(OH)_2$ at the iron electrode and $Ni(OH)_2$ at the nickel electrode. The rate of self-discharge could be as high as 8–10% of the nominal capacity per day at operational temperature of 40 °C [24]. Accordingly, sealed Ni–Fe cells with recombinant catalyst will be attractive, particularly, for float-charge applications.

The cells were also subjected to charge–discharge cycle-life test at C/5 rate and the data are shown in Figure 9(a), which reflect little loss in the nominal capacity of the Ni–Fe cell equipped with the catalyst. By contrast, the cell without catalyst showed monotonic fall in its capacity with cycle number (Figure 9(b)). These data clearly reflect the superior performance of the sealed Ni–Fe cells equipped with the recombinant catalyst in relation to those with no recombinant catalyst.

Typical charge–discharge data for the 6 V/1 Ah Ni–Fe battery at C/5 rate at 25 °C are shown in Figure 10. The battery was cycled for 25 cycles and found to retain its nominal capacity. Subsequently, the battery

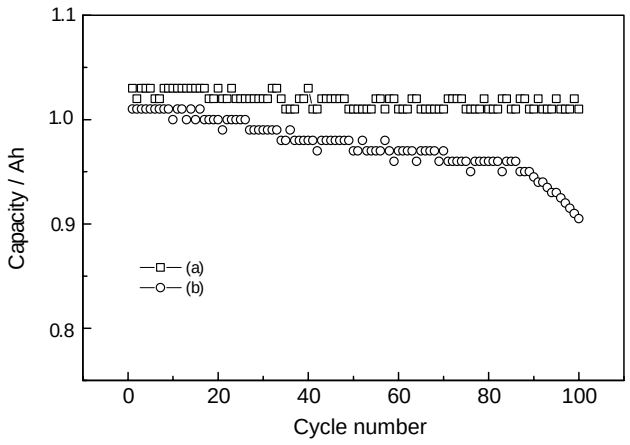

Fig. 9. Cycle-life data obtained at C/5 rate at 25 °C for (a) 1.2 V/1 Ah starved-electrolyte sealed Ni–Fe cell, and (b) 1.2 V/1 Ah starved-electrolyte vented Ni–Fe cell.

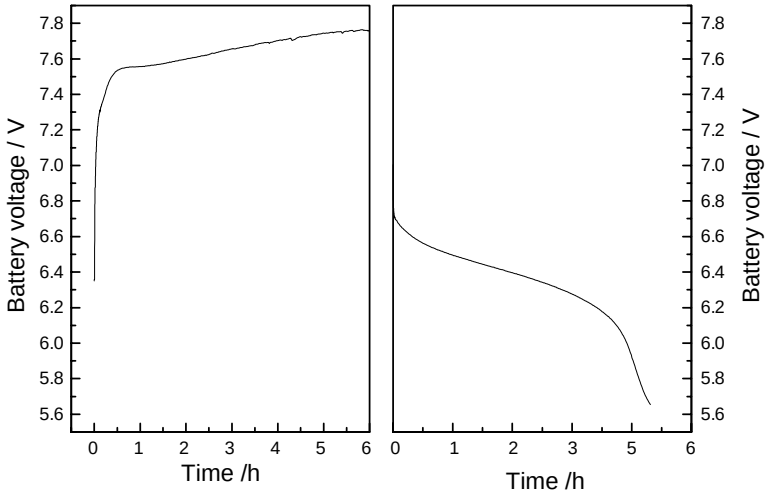

Fig. 10. A typical C/5 rate galvanostatic charge–discharge data for the 6 V/1 Ah starved-electrolyte sealed Ni–Fe battery at 25 °C.

was fully charged at C/10 rate followed by its discharge at C/5 rate (Figure 11). The battery was then kept under float charge for 100 h at C/10 rate followed by a discharge at C/5 rate (Figure 11). The capacity difference between the 26th and 27th discharge cycles was found to be only about 4% (see inset to Figure 11). These data further support that the Ni–Fe cells/batteries can be effectively employed for float-life applications, with little loss in their nominal capacity over prolonged durations.

4. Conclusions

A novel sealed, starved-electrolyte Ni–Fe battery was developed employing a recombinant catalyst and tested under various operational conditions. The faradaic efficiency of the constituent cells at 25 °C was found to be about 60% at C/5 rate. The discharge capacity values of the constituent cells at C/10 and C/2 rates at 25 °C with regard to their nominal discharge capacity at C/5 rate were observed to be 120 and 75%, respectively. At 40 and −20 °C, the discharge capacity values of the constituent cells with regard to their nominal capacities at 25 °C were found to be 97 and 12%, respectively. The self-discharge rate for the cells was found to be about 1% per day. The battery seems to be most adequate for float-charge applications in off-shore platform and petrochemical industries.

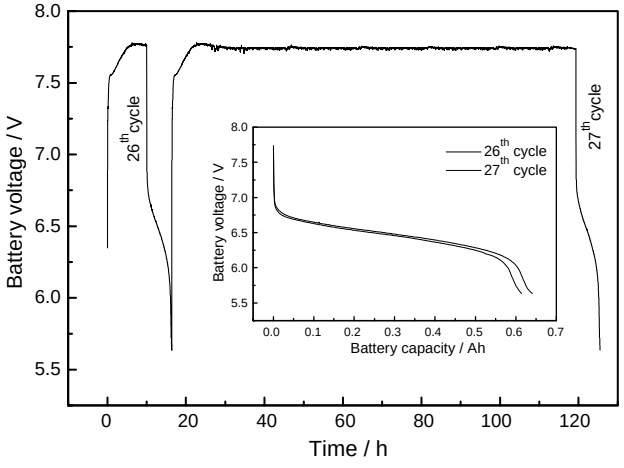

Fig. 11. Discharge data subsequent to 100 h of galvanostatic charging at C/10 rate for the 6 V/1 Ah starved-electrolyte sealed Ni–Fe battery at 25 °C.

References

1. W. Jüngner, Swedish Patent, 10,177,1899.
2. T.A. Edison, British Patent, 20,960,1900.
3. D. Linden and T.B. Reddy (eds), 'Hand Book of Batteries', 3rd edn (McGraw-Hill, New York 2002).
4. S.U. Falk and A.J. Salkind, 'Alkaline Storage Batteries' (Wiley, New York, 1969).
5. G.W. Vinal, 'Storage Batteries', 4th edn (John Wiley and Sons, New York, 1955).
6. C.A. Vincent and B. Scrosati, 'Modern Batteries' (Arnold, London, 1997).
7. R.M. Dell and D.A.J. Rand, 'Understanding Batteries' (Royal Society of Chemistry, Cambridge, UK, 2002).
8. D.A.J. Rand R. Woods and R.M. Dell, 'Batteries for Electric Vehicles' (Research Studies Press, England, 1998).
9. M. Cook and H. Morrow, *Met. Bull.* April 1992.
10. S. Sathyanarayana, The Nickel–iron Storage Batteries – A Status Report and Techno-Economic Survey for India, National Research Development Council, India, 1983.
11. L. Ojefors, Studies on the Alkaline Iron Electrodes, Swedish National Development Co., Royal Institute of Technology, Stockholm, 1975.
12. K. Vijayamohanan, T.S. Balasubramanian and A.K. Shukla, J. Power Sources, **34** (1991) 269.
13. O. Lindström, *in* D.H. Collins (Ed.), 'Power Sources 5' (Academic Press, London, 1975), p. 283.
14. J. Labat, J.C. Jarrousseau and J.F. Laurent, *in* D.H. Collins (Ed.), 'Power Sources 3' (Oriel Press, Newcastle upon Tyne, UK, 1970), p. 283.
15. F.C. Anderson, *J. Electrochem. Soc.* **99** (1952) 245C.
16. J. Cerny, J. Jindra and K. Micka, *J. Power Sources* **45** (1993) 267.
17. K. Vijayamohanan, PhD Thesis, Indian Inst. Sci. (1989).

18. T.S. Balasubramanian, PhD Thesis, Indian Inst. Sci. (1994).
19. M.K. Ravikumar, PhD Thesis, Indian Inst. Sci. (1998).
20. K. Vijayamohanan, A.K. Shukla and S. Sathyanarayana, *Indian J. Technol.* **24** (1986) 430.
21. K.C. Patil, S.T. Aruna and S. Ekambaram, *Curr. Opin. Solid State Mater. Sci.* **2** (1997) 158.
22. B. Hariprakash, P. Bera, S.K. Martha, K.C. Patil, S.A. Gaffoor, M.S. Hegde and A.K. Shukla, Indian Patent, April 2000.
23. B. Hariprakash, P. Bera, S.K. Martha, S.A. Gaffoor, M.S. Hegde and A.K. Shukla, *Electrochem. Solid-State Lett.* **4** (2001) A23.
24. T.S. Balasubramanian, M.K. Ravikumar and A.K. Shukla, *J. Power Sources* **51** (1994) 27.
25. A.K. Shukla, S. Venugopalan and B. Hariprakash, *J. Power Sources* **100** (2001) 125.
26. M.K. Ravikumar, T.S. Balasubramanian and A.K. Shukla, *J. Power Sources* **56** (1995) 209.